Combustion of Low-heating-value Fuel in Combustor of Gas Turbine with Swirler

Jai-Houng Leu,[1] Yan-Zuo Chang,[2*] Tian-Syung Lan,[2]
Shi-Dong Li,[2] and Ho-Sheng Chen[2]

[1]Shandong Polytechnic, No. 23000, Jin Ten East Road, Jinan City, Shandong Province 250104, China
[2]College of Mechatronic Engineering, Guangdong University of Petrochemical Technology,
Maoming Guangdong 525000, China

As the concern about environmental problems and overuse of fossil fuels increases, alternative fuels with low heating values have been gaining much attention. Combusting the fuels requires modified gas turbines in terms of design and operation parameters. In this study, we aim to find appropriate parameters for designing gas turbines that combust low-heating-value fuels (LHVFs) through computer simulation. The results indicate that the jet penetration depth, inlet gas coefficient, and jet flow direction in the wall jet inlet require adjustment in the combustor design. The simulation shows that a pair of small vortices form in the front of the dome region. The length of the recirculation flow is only $0.18D$ (D: inlet diameter of the combustor), which does not significantly affect the flame-holding ability. The results also reveal that the strength and size of the recirculation flow in the primary combustion zone must be increased as the center of the flow moves to the liner wall. The high-temperature zone must also be close to the liner, and the center of the recirculation flow must be close to the liner wall. As a result, the combustion efficiency of LHVFs in the newly designed combustor is improved by 47% from that of a conventional combustor. The results of this study are expected to lead to new innovative designs of combustors of LHVFs that save resources and reduce pollutant emission.

1. Introduction

Low-heating-value fuels (LHVFs) have a lower calorific value (generally less than 9000 kcal/m^3) than fossil fuels such as natural gas, coal, and petroleum. As they are chemically synthesized, LHVFs include impurities such as carbon particles and H_2S. There are many kinds of LHVFs such as biomass, organic gases, and synthesized gases.[1] As LHVFs have less effect on global warming, there have been many efforts to replace fossil fuels with LHVFs. Consonni and Larson reported that around 10% of the total electricity of the USA is provided from power generation units using LHVFs.[2] However, using LHVFs requires modification of existing combustion systems or gas turbines to improve combustion efficiency due to their low calorific values as most LHVFs are in gaseous form.

A gas turbine with a combustion chamber is widely used to burn LHVFs as it gives better and easier control than modified combustion systems. A gas turbine is suitable for enhancing the combustion efficiency when using LHVFs as the combustion can be controlled in multiple parts of the turbine. For appropriate combustion efficiency, a swirler is needed in a gas turbine. A swirler is generally used with open flame injectors in the internal combustion engines and gas turbines of jet engines of aircraft. A swirler in a gas turbine mixes an LHVF and air and creates a flame retention effect that extends the residence time of the mixture. Thus, gas turbines with swirlers effectively regulate combustion and improve its efficiency.

Birkby *et al.* presented a series of computational fluid dynamics simulations of a Royce Trent industrial combustor by using the McNEWT unstructured code.[3] The entire combustion chamber geometry including the premixing ducts, fuel injectors, and discharge nozzle was represented. Their results provided useful information on the operation of the combustor and values for combustion analysis such as the non-reacting flow field, the mixing ratio of fuel to air, and the combustion process under different operating conditions. Syred developed a gas turbine combustor with a strong precessing vortex core under an isothermal condition and suggested the equivalence premixing number.[4] These studies and others indicated the feasibility of gas turbine swirl burners with helical coherent structures and radial axial eddies, which generate alternating rich and lean combustion to reinforce combustion under the Rayleigh criteria. However, the results were for conventional fossil fuels, not for LHVFs.

An LHVF in a gas turbine must be combusted on a large scale with precise control of the related parameters. Therefore, designing the combustion chamber (combustor) of the gas turbine requires adjustment and modification based on numerical simulations to find the design principles and parameters, along with experiments to verify the combustion efficiency and process. As a gas turbine is complicated and expensive, these simulations and experiments are critical for the practical and efficient use of LHVFs. In the experiments, state-of-the-art sensor technology is needed to accurately measure the temperature and the flow rates of air, the fuel, and the mixture. The sensor technology used in the experiments includes thermocouples for high-temperature measurement, an economizer with a micrometer for flow rate measurement, and a signal processor for calibrating the signals from the sensors. The essential information on the effects of LHVFs and air nozzles is then obtained by using the measured data for the gas turbine combustor.

Alternative fuels including LHVFs have lower calorific values than fossil fuels, so they emit less pollutants. However, existing commercial combustion systems must be modified to improve the combustion efficiency of alternative fuels. In particular, turbine combustors need modification or redesigning. The turbine combustor is an essential and expensive component of a combustion system, although it is relatively easy to modify. Sensors play an important role in the modification, as precise and accurate data are critical for designing the swirler of the gas turbine in the combustor, and a feasible design can be obtained by numerical calculation based on the data from sensors. Therefore, we investigate in this study the parameters of a gas turbine for combusting LHVFs, such as the air distribution, fuel composition, swirl number, and wall-cooling flow, by using data collected from sensors to visualize the flow fields of inlet gases and simulate the combustion. The results will be helpful for future research on improving the designs

of combustors for a variety of LHVFs, and this study provides an appropriate method for performing simulations and adjustments to enable the use of a wide range of LHVFs.

2.   Methods

2.1   Low-heating-value fuels

The heating value of the gasified coal used as the LHVF (about 6300–7200 kcal/m^3) in our experiments was estimated to be about 70–80% of that of coal. Methane was also tested for reference. The design parameters were adjusted according to the results of a numerical simulation of combusting the LHVF to manufacture the newly designed combustor. The combustion efficiency of the LHVF was estimated by comparing the experimental parameters obtained in the newly designed combustor and a conventional combustor.

2.2   Combustor

The combustor proposed by Leu[5] was used for the experiment (Fig. 1), which is used for the non-closed reciprocating internal combustion of LHVFs. The diameter and length of the combustor are 60 cm, and the length of the rear (secondary) combustor is 30 cm including the 10 cm rear retraction. The combustor has air and gas swirlers, a main combustion chamber (main jet), and a rear combustion chamber (secondary jet). The experiments were carried out for 24 different scenarios with heating values from 6.7 MJ/m^3 (1600 kcal/m^3) to 25.5 MJ/m^3 (6300 kcal/m^3) and conditions from no swirling to a strong vortex (swirl number of 18.75).

2.3   Measurement

The influence of the air-to-fuel ratio on the adiabatic flame temperature was investigated using STANJAN software.[6] Information on the combustion temperature in various zones of the
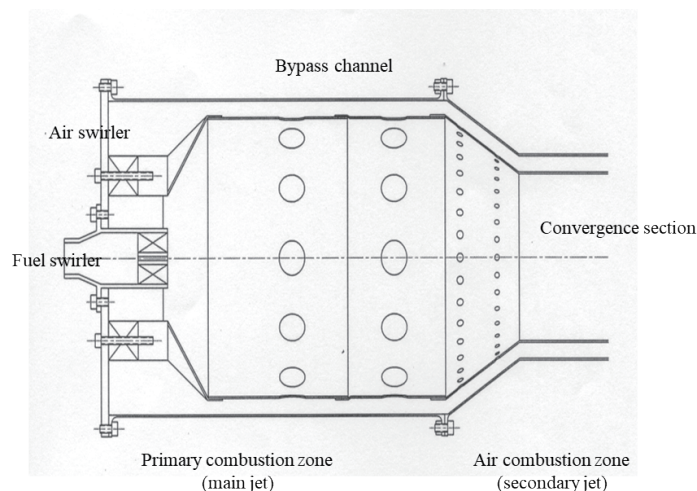

Fig. 1.   Design of the combustor.

flow field was obtained from the airflow distribution. The results provide basic information for velocity forecasting and thermal conduction analysis. Considering the overall air-to-fuel ratio of the original combustor, the average temperature in the combustor outlet was set to be lower than 427 °C.[5] Table 1 illustrates the inlet conditions used in the simulation analysis of the flow field in the combustor.[7] A K-type thermocouple (MAX6675) was used to measure the temperature in three-dimensional traversing tests. The flow rates of air and fuel were measured using a far-IR economizer (CEM-06). A piezoelectric pressure sensor (SEN09376) was set up to measure the pressure. The signal from the sensors was calibrated using the Bernoulli and momentum equations, and the related parameters were estimated after detection and comparison.

For a fixed size of the combustor housing, the flame tube height is chosen after evaluating the overall combustor performance. Increasing the ratio (K) of the flame tube and housing areas decreases the flow rate in the tube but increases the residence time, which improves space utilization. Reducing the pressure difference of the air through the hole is unfavorable for the mixing of air and fuel. Therefore, the optimal value of K is obtained using the following equation:[8]

$$\frac{\Delta P_L}{q_{PZ}} = 1 + \frac{T_2 K^2}{T_{PZ} m_{PZ}} \left\{ \frac{\Delta P_{3-4}}{q_{ref}} - \frac{\left(1 - m_{sn}\right)^2 + \lambda \left[r^2 \left(1 - K\right)^2 - 1 \right]}{\left(1 - k\right)^2} \right\}, \qquad (1)$$

where T_{pz} is the temperature in the main combustion zone, m_{pz} and m_{sn} are the air ratios in the main combustion zone and vortex mixer, respectively, r is the ratio of the housing area to the section area, and λ is the coefficient of diffuser pressure loss. In our preliminary design, m_{pz} = 0.227, m_{sn} = 0.103, r = 8.48, and λ = 0.18.

3.   Results and Discussion

Table 2 shows the specifications for a design of the combustion system obtained using the equation proposed by Chomiak *et al.*[9] Air entering the primary combustion zone is acted on by a swirler to produce a tangential velocity. To avoid energy loss caused by sudden expansion, the front-end panel angle was set at 55°. Using the law of momentum conservation, the swirl number

Table 1
Inlet conditions for flow-field analysis in the combustor.

Inlet	Air swirler	Fuel gas	Primary cooling jet	Penetration jet	Main jet	Secondary cooling jet
Mass (kg/s)	0.0334	0.019962	0.0062	0.0921	0.122	0.0096
Ratio (%)	12.7	100	2.5	32.2	46	3.6
Velocity component (m/s)	u = 7.52 w = 12.5	u = 5.744 v = 4.022	v = −105.05	v = −15.05	v = −15.05	v = −11.0

Penetration jet: jet flowing from the bypass into the combustion chamber
Main jet: jet penetrating into the main combustion chamber
Secondary cooling jet: jet flowing into the post-combustion chamber (mainly for cooling)

Table 2
Design specifications of the combustion system.

Item	Category	Specification	Description
Work	Fuel heating value	>1500 kcal/m^3	Derived from tire gasification
	System output power	10 kW	Same as the original system
	Service life	>500 h	—
Operability	Starting	Temperature is 10–40 ℃	Spark plug ignition
	Deficient boundary	Not important	Runs at the design point
Performance	Efficiency of combustion	>96%	—
	Drop in pressure	<9% total pressure	—
	Outlet temperature coefficient	<0.4	Can be slightly raised
Construction	Can shape	—	Similar to the original system
	Size	Outlet adapted to system interface	No limit in diameter
	Weight	No limit	Ground-mounted equipment
	Fixing method	Similar to original system	Easy to dismantle
	Assembly	Modular design adopted	Facilitating later adaptation
Pollution emission	Smoke and fog	None	—
	NOx	Not considered	—

S (the ratio of tangential momentum flux to axial momentum flux) of inlet air was estimated to be larger than 0.6, which would cause vortex breakdown. To avoid this, deflected gas was introduced and mixed with auxiliary gas/air to prevent damage caused by the central recirculation flow. The air jet position and distribution rate were closely related to the outlet temperature of the air. The axial distance between the main and penetration jets was 0.62R (R: radius of the combustor). Table 3 illustrates the inlet conditions of the air and fuel gas at different positions under a full load.

Table 4 shows the heating values and swirl numbers for different mixtures of the LHVFs. The boundary conditions (vortex intensity) were set on the basis of numerical simulation results.

The governing equations for the airflow in the combustor were proposed by Fukue *et al.*[1] The commercial software STAR-CD, a model for simulating turbulence, allows various scenarios in practical application. Although its accuracy is low due to strong numerical diffusion, it is possible to obtain a convergent solution for a combustor design. Thus, we used the STAR-CD SIMPLE simulation model of combustion in the solution process.[10]

The combustion system has a denser grid in the axial direction near the airflow field as air and fuel have a strong mixing shear flow. The jet flow of the inlet tends to be denser to avoid false diffusion and underestimation of the penetration depth. Also, the cooling jet that forms the airflow field structure near the outlet has a denser grid in the axial direction. In the tangential direction, the grid is divided into equal angles with three boundary conditions for the inlet, the outlet, and the cycle. Here, the average temperature, velocity, intensity, and concentration are measured, and a non-axial gradient of the combustor is assumed for the outlet condition. Finally, the conditions of the cycle at the end of the convergence section are established.

The recirculation flow moves along the centerline of the primary combustion zone. The air-fuel mixture at a high temperature reversely flows to the central area of the fuel gas nozzle. The

Table 3
Inlet conditions of air and fuel gas at different positions under full load.

Inlet	Fuel gas	Air swirler	Main jet	Penetration jet	Primary cooling jet	Secondary cooling jet
Mass (kg/s)	0.019962	0.0334	0.122	0.0921	0.0062	0.0096
Percent (%)	100	12.7	46	32.2	2.5	3.6
Velocity component (m/s)	$u = 5.744$ $v = 4.022$	$u = 7.52$ $w = 12.5$	$v = -15.05$	$v = -15.05$	$v = -15.05$	$v = -11.0$

(u, v, and w: velocity components in x-, y-, and z-directions, respectively)

Table 4
Boundary conditions and heating values of different simulation cases.

Heating value (MJ/m^3)	Swirl number				
	0	6.25	9.375	12.5	18.75
6.7	LHV02	LHV03	LHV24	LHV01	LHV04
11.8	None	None	None	LHV05	None
15.4	LHV10	LHV14	None	LHV06	LHV18
18.9	LHV11	None	None	LHV07	LHV19
25.5	LHV12	LHV16	None	LHV08	LHV20

main vertical jet does not appear in each tangential profile and the high-temperature mixture bypasses the main jet and the released downstream flow, as shown in Figs. 2(A)–2(D).

Owing to the staggered penetration and the main jet, a high temperature occurs on the leeward side of the main jet. A small-scale recirculation flow may cause weak flame holding. To reduce this phenomenon due to the high temperature, the combustor adopts wall jet cooling.

Figure 3 shows that the high-temperature areas are limited to the primary combustion zone and do not appear in the middle zone or near the wall of the combustor. The primary combustion zone produces two small recirculation cells with low strength. The fresh air of the main jet cannot fully return to the primary combustion zone and mixes with the fuel gas, resulting in an inadequate load in the primary combustion zone.

As shown in Figs. 2 and 3, there is a recirculation flow along the centerline of the primary combustion zone. The mixture at a high temperature reversely flows to the central area of the fuel gas nozzle, which provides an effective ignition source and causes the front wall surface of the combustor to have a high temperature. The temperature contours reveal that the highest temperature of the combustion is 1900 °C. The temperature of the mixture is 100 °C higher than that of the adiabatic flame at the same inlet temperature and pressure for the conventional combustor according to the combustion simulation. The main vertical jet does not appear in each tangential profile as the high-temperature mixture bypasses the main jet and releases the flow downstream [Figs. 3(a) and 3(d)]. Thus, high-temperature areas also appear in the middle zone. Owing to the staggered jet, these high-temperature areas are separated by the penetration jet. On the leeward side of the main jet, a small-scale recirculation flow causes a weak flame. As shown in Fig. 2(B), the fluid at a high temperature is separated by the penetration jet and extends downward to the liner. This may lower the outlet temperature.
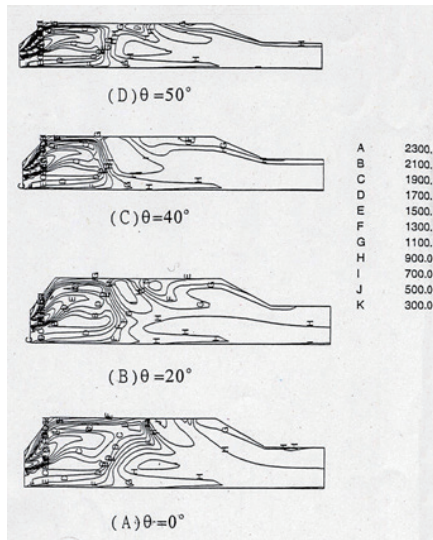
Fig. 2. Temperature contours of different tangential profiles (A to K represent different temperatures in Kelvin).
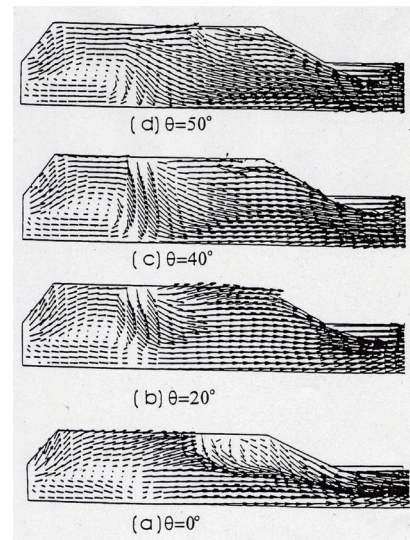
Fig. 3. Velocity diagrams of different tangential profiles.

To solve the problem of the high temperature, the combustor adopts the method of cooling the wall with the jet as a high temperature occurs near the wall. Although the cooling jet decreases the temperature significantly, the problem may not be solved; as the highest temperature reaches 1900 °C near the front wall of the combustor, the temperature of the wall can be over 700–800 °C, which exceeds its temperature limit. Thus, the temperature factor is set as 0.3 to give a temperature limit of 570 °C (1900 °C × 0.3 = 570 °C).[5]

The streamlines in the primary combustion zone obtained by flow visualization are shown in Fig. 4. Two groups of streamlines move around the inlet and flow back behind the rear of the inlet (Fig. 5). This is presented using the streamlines on the peripheral wall in Fig. 4.

The secondary recirculation flow moving upstream flows back and occupies most of the front dome region (Fig. 5). The recirculation structure in front of the dome region represents the main flame held in the side-inlet ramjet combustor. The flow moving into the front of the dome region coincides with the outer flow of the secondary recirculation flow from the primary recirculation flow. Owing to the high momentum of the inlet gas flow, the recirculation flows from the front of the dome region cannot disturb the inlet jet flow and cause vortex shedding. These flows are forced to flow through the passage between the two inlets. The secondary recirculation flow interferes with the primary recirculation flow. They interact with each other after temporary vibration, and then, come to balance to form a pair of vortices above and below the centerline almost symmetrically in the reverse direction (as shown in Fig. 5). These vortices are smaller than those in the front of the dome region. The length of the recirculation flow is only 0.18D (D: inlet diameter of the combustor) and its structure does not affect the flame-holding ability.

The characteristics of the recirculation flow in the swirler of the combustor are different from those of the shedding vortex behind the bluff bodies. The outer flow from the primary
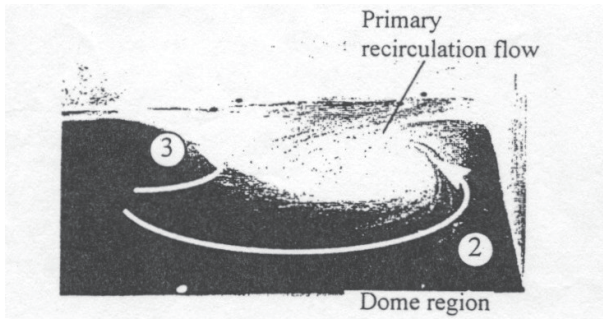
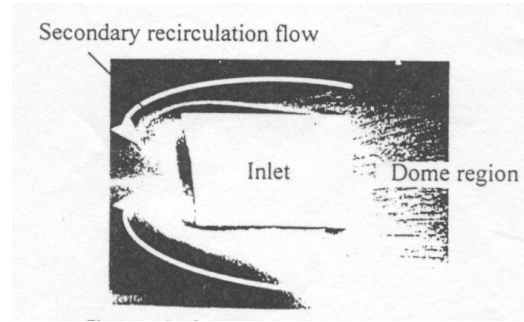Fig. 4. Primary recirculation structures in the combustor.

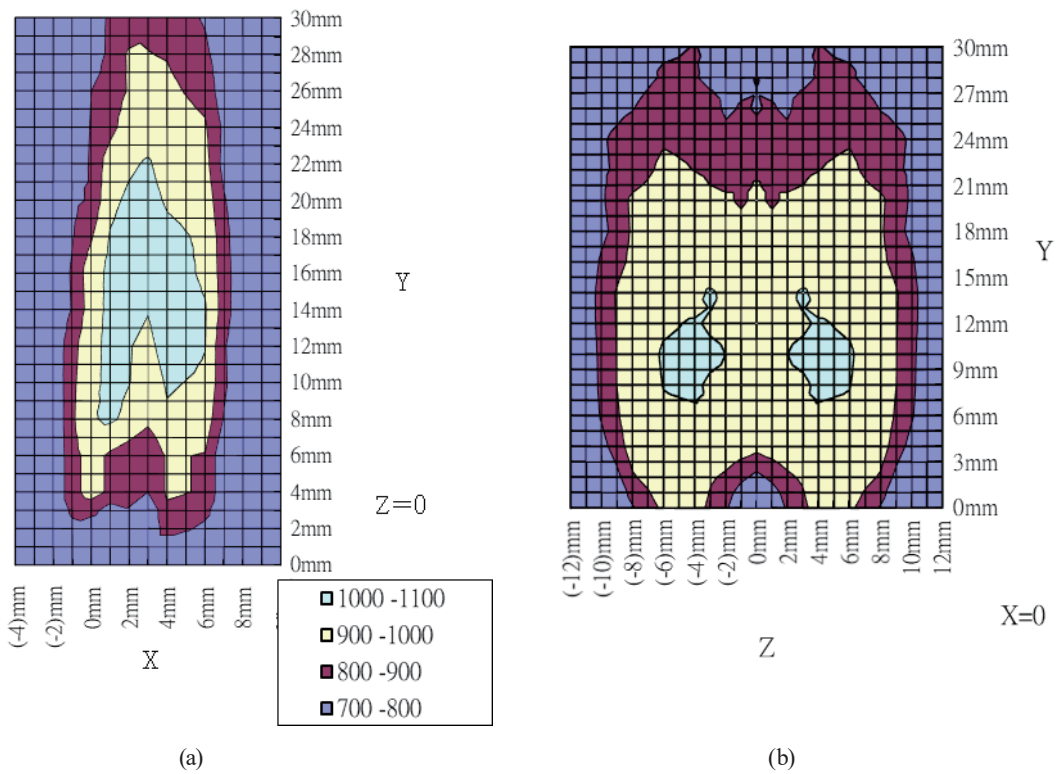Fig. 5. Pair of recirculation flows behind the inlet.

(a)

(b)

Fig. 6. (Color online) Temperature profiles (in °C) at central lines for air at Reynolds number of $Re = 195$ and CH_4 at $Re = 290$. (a) X–Y plane at $Z = 0$. (b) Y–Z plane at $X = 0$.

recirculation zone through the two jet columns is not obstructed by the inlet gas flow. Therefore, combustion instability due to the vortex-shedding process does not occur.

Figure 6 presents the temperature profiles obtained from the combustion simulation between 900 and 1100 °C. They show a long and unsaturated flame with a lower combustion efficiency for the LHFVs than that of methane. The distribution of the peak temperature of the air is narrower than that of methane. This is also clearly observed under a lean combustion condition. The mass and heat transfer increase with the momentum ratio of the penetration jet to the main jet.

The heating value of a fuel varies significantly with its biological source and manufacturing process. Many studies have focused on the integrated gasification combined cycle (IGCC) [11] or the topping cycle.[12] The overall combustion efficiency of the latter is higher than that of conventional coal combustion. The heating value of gasified coal is estimated to be about 70–80% of that of coal. However, the results of this study showed that the combustion efficiency of LHFVs in the newly designed combustor was improved by 47% from from that of the conventional combustor.

4.   Conclusions

A newly designed combustor for an LHVF was first optimized by numerical simulation. Then, the operation of the combustor was validated by flow visualization, combustion simulation, and experimental detection. The processes of the designed combustor were established for the LHVF of gasified coal. These processes can be applied to other LHVFs such as gasified rice husks and sawdust.

The temperature distribution of LHVFs in a combustor shows improved flame-holding ability with increasing jet penetration depth. Improving the structure of the recirculation flow in the primary combustion zone requires blocking of the effect of the wake zone as the decisive factor. The primary recirculation flow fills the front of the dome region. However, the size of the flow is much smaller than that in the front of the dome region. The vortex in the swirler of the combustor flows continuously without being processed in a shedding cycle. To validate and improve the current design concept, the optimized values for the fuel composition, swirl number, the configuration of the wall-cooling flow, and a jet flow with high penetration strength for the pre-mixing combustion must be applied to the air distribution. The results of our experiment indicate that increased penetration of the flame is disadvantagous for the mixing rate of air to fuel in the inner flame. As the fuel and air jets are located on the same side, the main reaction occurs in the fuel. Thus, the momentum ratio significantly influences the combustion efficiency. The results in this study show that the LHFVs in the newly designed combustor had higher combustion efficiency than in a commercial combustor. Even though the heating value of gasified coal is about 70–80% of that of coal, the combustion efficiency of LHVFs in the newly designed combustor was improved by 47% from that in the conventional combustor.

References

1   J. Fukue, S. Mandai, and. M. Inada: Aerothermodynamics in Combustors, Part V (Springer-Verlag, Berlin, 1991). https://doi.org/10.1007/978-3-642-84755-4

2   S. Consonni and E. D. Larson: J. Eng. Gas Turb. Power **114** (1992) 665. https://doi.org/10.1115/1.2816677

3   P. Birkby, R. S. Cant, W. N. Dawes, A. A. J. Demargne, P. C. Dhanasekaran, W. P. Kellar, N. C. Rycroft, A. M. Savill, R. L. G. M. Eggels, and I. K. Jennions: Proc. 2000 Turbo Expo (2000). https://doi.org/10.1115/2000-GT-0131

4   N. Syred: Prog. Energy Combust. Sci. **32** (2006) 93. https://doi.org/10.1016/j.pecs.2005.10.002

5   J. H. Leu: J. Inf. Opt. Sci. **31** (2010) 1321. https://doi.org/10.1080/02522667.2010.10700030

6   W. C. Reynolds: Stanford University, California (1986). https://shepherd.caltech.edu/EDL/PublicResources/sdt/refs/STANJAN_1986_Reynolds.pdf

7   X. Feng: Adv. Mat. Res. **268–270** (2011) 494. https://doi.org/10.4028/www.scientific.net/AMR.268-270.494.

8   A. M. Starik, A. M. Savbel'ev, N. S. Titova, and U. Schumann: Aerosp. Sci. Technol. **6** (2002) 63. https://doi.org/10.1016/S1270-9638(02)01150-1

9   J. Chomiak, J. P. Longwell, and A. F. Sarofim: Prog. Energy Combust. **15** (1989) 109. https://doi.org/10.1016/0360-1285(89)90012-9

10 P. J. Jones and G. E. Whittle: Build Environ. **27** (1992) 321. https://doi.org/10.1016/0360-1323(92)90033-L

11 J. S. Kapat, A. K. Agrowal, and T. Yang: J. Eng. Gas Turb. Power **119** (1997) 20. https://doi.org/10.1115/1.2815551

12 W. F. Domeracki, T. E. Dowdy, and D. M. Bachovchin: J. Eng. Gas Turb. Power **119** (1997) 27. https://doi.org/10.1115/1.2815558